Segmentation algorithm of coal slurry foam with double-point directional extension based on the improved FCM clustering algorithm

ZiHao Wu [1], XianWu Huang [1], HaiLi Shang [2], YuHong Zhao [3]

[1] School of Information Engineering, Inner Mongolia University of Science & Technology, Baotou, China;

[2] Key Laboratory of Coal Processing and Efficient Utilization, (China University of Mining and Technology), Ministry of Education, Xu Zhou China;

[3] School of Information Engineering, Inner Mongolia University of Science & Technology, Baotou, China;

Corresponding author: huangxianwu1983@163.com (XianWu Huang)

Abstract: In flotation production, the visual surface information of the flotation foam reflects the flotation effects, which are closely related to the flotation conditions and directly reflect the degree of mineralization of the foam layer. In this study, it was proposed a novel and efficient segmentation algorithm to extract the edge information of slime bubbles, as the boundaries are typically blurred and difficult to segment, due to the slime bubbles sticking to each other in the slime flotation foam image. First, the improved clustering algorithm and image morphology operation were used to extract the edges of the foam spots. Second, the image morphological operations were used as a starting point to look around the foam edge points. The pseudo-edge points were then removed using a region and spatial removal algorithm. Finally, the foam edges were extracted using the double-point directed expansion algorithm. A new criterion was proposed for segmentation effect determination based on the particularity of the segmented object. The feasibility and effectiveness of the foam segmentation method were investigated by comparative experiments. The experimental results showed that the proposed algorithm could obtain the foam surface properties more accurately and provide effective guidance for flotation production.

Keywords: flotation, slime foam segmentation, FCM clustering algorithm, double-point directional extension, segmentation effect judgment standard

1. Introduction

Froth flotation consists of a separation method based on the differences in hydrophilicity and hydrophobicity of a mineral surface (Aldrich et al., 2000; Kalyani et al., 2007). The characteristic information of a foam surface can be closely related to the flotation state, and these visual features can provide important operational guidance for flotation production, ensuring the stable operation of flotation production. So far, this task has been used to adjust operations by manually observing the foam state, resulting in low labor productivity and high labor intensity of workers (Kaijun et al., 2010). Due to large subjectivity and arbitrary among operators, there is no objective standard for foam assessment, which can lead to frequent fluctuation in the flotation production index and low mineral resource utilization. Today, with the increasing scarcity of high-grade mine resources, it is more difficult to effectively implement the manual operation of flotation production, especially when the flotation source has a complex composition and a low mineral grade. To overcome these issues, machine vision and intelligent control technology based on foam characteristics have been used to monitor flotation production (Vallebuona et al., 2008).

Applying machine vision (Aldrich et al., 2010; Nakhaei et al., 2019; Deniz et al., 2022) to the flotation process and analyzing the flotation froth image using digital image processing technology (Wang et al., 2020) can be used to objectively describe the froth state (Murphy et al., 1996; Wang et al., 2001). In the flotation process, the visual features, including the foam size (Cho et al., 2002), color, texture, and flow rates (Park et al., 2022) of the froth surface can be closely related to the process indicators, working

conditions, and operating variables, which can be used as an important basis for determining the effect of separating operations of the mine. Therefore, the accurate extraction of foam image features is considered a prerequisite for the machine vision-based monitoring of float production processes. Correlation analyses between the characteristics of the foam and the key process parameters of on-site flotation have been conducted, and mathematical modeling has been used to predict the pulp ash content, and dosage of various agents (Jose et al., 1992; Jian et al., 2008; Liu et al., 2011; Aryasuta et al., 2022), and the tail coal ash content in the current foam state, which could be used to guide subsequent flotation production.

In recent years, considerable research has been conducted on foam segmentation. The watershed algorithm is a common segmentation method (Ng et al., 2006; Cao et al., 2021; Zhou et al., 2022). Jing et al. (2017) proposed a watershed segmentation model based on bilateral filtering and contrast-limited adaptive histogram equalization to address the issues of high noise, low contrast, and bubble adhesion in foam images collected in the industrial field. Jun et al. (2020) proposed an improved watershed algorithm based on the 4-neighborhood similarity, which was applied to the k-means (Likas et al., 2003) initial clustering image to segment the target region. Edge detection (Ziou et al., 1998; Su et al., 2021; Jing et al., 2022). Wang et al. (2000) proposed a valley edge detection algorithm for foam images to segment the original image, comparing the foam edge to the valley edge to connect all edge points and achieve bubble segmentation (Wang et al., 2000; Bhondayi et al., 2022). Huifeng et al. (2011) improved the edge detection algorithm based on the foam pattern feature extraction method of the adaptive optimal valley bottom detection threshold of the adaptive particle swarm optimization algorithm; the inertial weight and acceleration factor of the particle swarm algorithm were set as a function of the global optimal fitness degree, and the bubble edge was obtained by the optimal valley bottom detection threshold. The texture spectrum (He et al., 1990; Backes et al., 2013; Deng et al., 2021). Yuan et al. (2018) proposed an image texture feature extraction algorithm based on the Gabor filter (Meng et al., 2021) and CS-LBP operator (Han et al., 2017) for the one-way nature of traditional texture extraction, transforming the extracted frequency components into the time domain to achieve texture extraction (Yuan et al., 2018). Luo et al. (2019) proposed a new PCA-based algorithm to extract the texture features of foam images by comprehensively considering the granular texture features on the surfaces of foam particles.

Due to the complexity of the industrial environment, the surface of a foam image collected in the field is rough, with considerable noise. In addition, the foam velocity is too fast, causing the image to blur, with numerous light spots and dark areas in the image, and the traditional segmentation algorithm has difficulty achieving a good segmentation effect. Therefore, considering the complexity of the above environment, a new segmentation algorithm for foam images was proposed in this work. After pre-treatment of the images collected from an industrial site, the foam features could be effectively extracted, and the main innovations of the algorithm were as follows:

(1) The improved FCM clustering algorithm was used to obtain the foam light spot region, and the image binarization and morphological operations were used to obtain the edge of the light spot. Subsequently, the edge of the light spot was used as a starting point to search for foam edge points around it, to form an edge candidate set.

(2) Considering the existence of the pseudo-edge point in the edge point set, in this work, we proposed a region and spatial removal algorithm to screen the pseudo-edge point in the edge point set and we eliminated the pseudo-edge points, generating a foam candidate point set.

(3) Considering the problem that the candidate point set was discontinuous and had difficulty expressing the characteristic information of the foam edge, a double-point directional extension algorithm was proposed to extract the foam edge.

Because the bubbles in the coal-slime foam images were glued to each other, the extracted edges were narrow and inconspicuous, making it difficult to accurately determine the feature extraction results using traditional segmentation criteria. Therefore, we proposed a new segmentation criterion for segmentation effect detection.

3

Physicochem. Probl. Miner. Process., 59(1), 2023, 158850

2. Foam image segmentation algorithm

2.1. Algorithm description

The characteristics of the slime flotation foam were as follows. (1) The uneven illumination caused numerous spots and dark areas to appear in the foam image. (2) The grey value inside the bubble was uneven. (3) The average grey value of the bubbles varied greatly in the different regions of the image. When an edge detection algorithm was applied to this image set, most of the light spot edges were delineated, while the bubble edges were lost.

The main reasons why classical image segmentation algorithms could not accurately segment foam images were as follows. (1) The uneven lighting caused the original image to appear in light spots and dark areas, and this effect was too severe. (2) Affected by the size of coal particles, the local reflected light was uneven, the greyscale changes in the foam surface were not sufficiently smooth, and the gradient changed significantly. (3) At the connection of the foam edges, a narrow and smooth plane appeared, and the gradient changed sharply, affecting the segmentation effect. (4) The light spot at the top of the foam was overexposed, and the grey gradient change of the edge of the top light spot was larger than the edge of the foam. The greyscale information of the foam image is shown in Fig. 1, where in Fig. 1 (b), the red circle marks the foam edge and the blue circle marks the reflective area of the saddle. Fig. 1 (c) shows the greyscale of the foam image, indicating that the greyscale variation gradient of the foam image was extremely large.

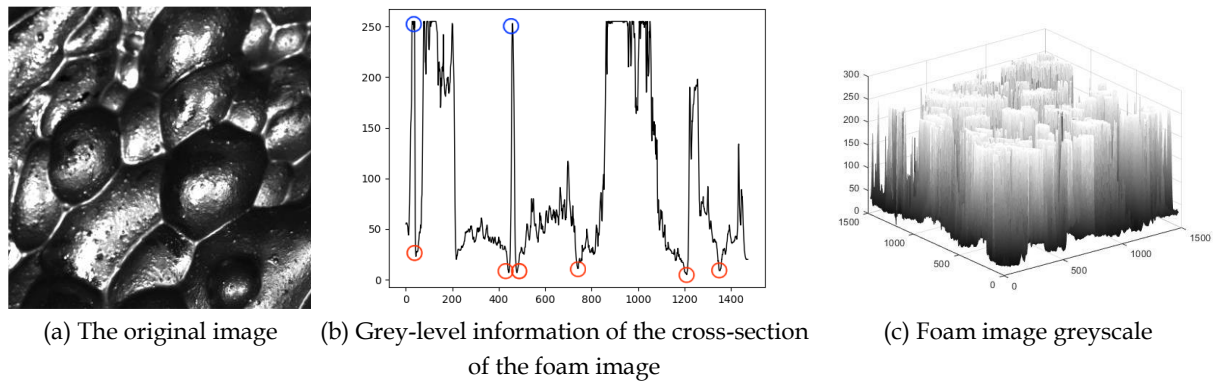| (a) The original image | (b) Grey-level information of the cross-section of the foam image | (c) Foam image greyscale |

Fig. 1. Grey-level information of the foam image

Considering the above features, in this study, it was proposed a new segmentation algorithm, whose steps are shown in Fig. 2. First, the raw images were pre-processed with Gaussian filtering to remove the image noise caused by the uneven size of the coal particles and illumination of the foam surface. Second, a modified FCM clustering algorithm was used to extract the foam light spot regions, and image binarization and morphological operations were performed to obtain the light spot edges. Using the edge of the light spot as a starting point, edge points were observed around it, forming an edge point set. The pseudo-edge points in the edge point set were then removed using the region and spatial removal algorithm to form a set of candidate points. Finally, based on the candidate point set of the foam edge, the double-point directional extension algorithm was used to complete the extraction of the foam edge. After completing image segmentation, the segmentation effect was detected by using the proposed segmentation criterion.

2.2. Image pre-processing

The foamy images collected at the float site were almost completely occupied by bubbles that adhered to each other. At the same time, locally reflected illumination was inhomogeneous due to the size of the coal particles, causing a non-smooth grey level of the foam surface and making it difficult to extract foam edge information. Therefore, it was necessary to pre-process the raw foam images to improve the accuracy of edge extraction. Experiments with various image preprocessing operations have shown that the Gaussian filter provides the best results. The specific results of the experiment are shown in Fig. 3, where the mean filtering was fast and the algorithm was simple; however, the noise could not be
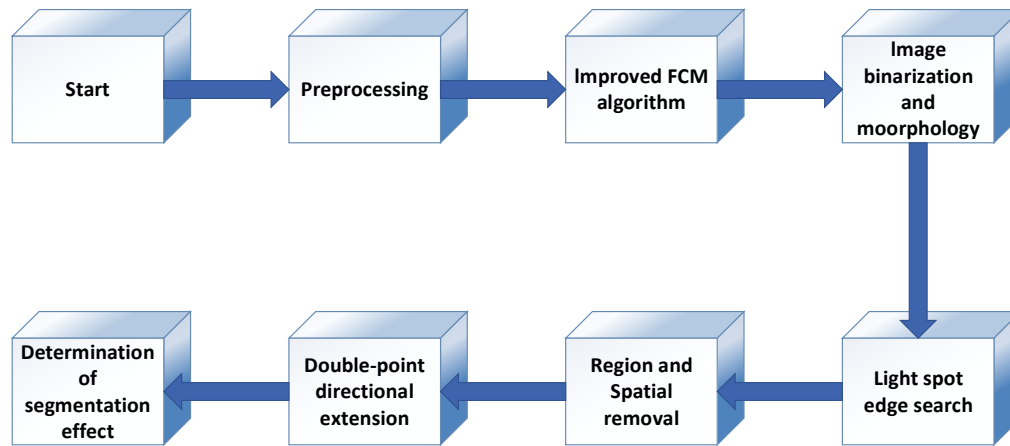
Fig. 2. Algorithm flow chart

removed and was only weakly reduced. Median filtering protected the sharp edges in the image, but the coal grain edge was sharper than the foam edge, which was eventually retained. Therefore, a Gaussian filter could be used to effectively obtain an ideal pre-processed image. Gaussian filtering consists of a simple and fast linear smooth denoising algorithm (Si et al., 2014; García-Fernández et al., 2021). A Gaussian filter was used to denoise the foam image, and while removing the noise, the details of the foam edges were preserved as much as possible. In this study, after pretreatment using this method, we observed almost no obvious particle bulges on the foam surface, and the bubble edges were obvious, which was helpful for subsequent segmentation operation.
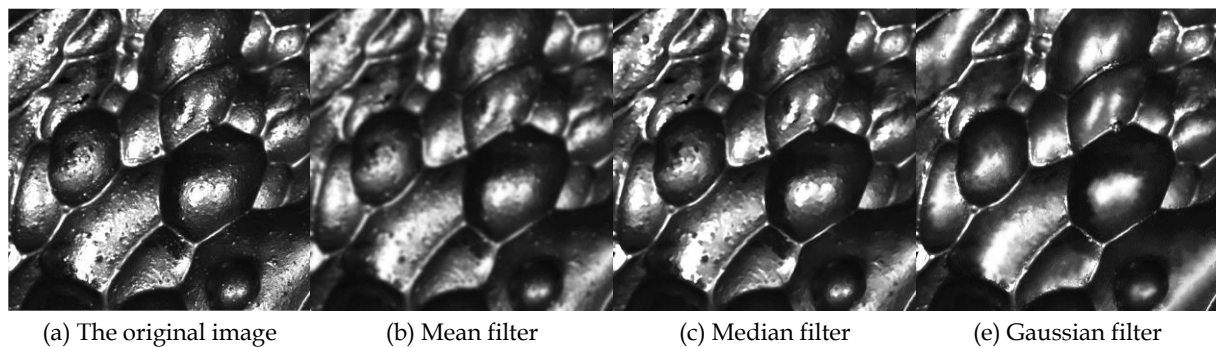
(a) The original image   (b) Mean filter   (c) Median filter   (e) Gaussian filter

Fig. 3. Comparison of the preprocessing effect

2.3.   Image segmentation

2.3.1. Foam edge point acquisition

First, an improved FCM clustering algorithm was used to obtain the foam spot region of the preprocessed image, and the image binarization and morphological operations were performed to obtain the spot edge, where we used the edge of the light spot as the starting point to search for surrounding edge points to form a foam edge point set. The steps were as follows:

- **Step 1** The improved FCM clustering algorithm (Uplaonkar et al., 2021; Karunkuzhali et al., 2022; Lavanya et al., 2022) was used to obtain the foam light spot of the pre-processed image.
- **Step 2** The image binarization (Kim et al., 2017; Feng et al., 2022) operation was performed on the acquired feature layer of the spot area, and the grey value information was divided into two parts, namely, the light spot and the background, where a morphological operation (Jones et al., 1994; Chudasama et al., 2015) was performed on the light spot to obtain the edge of the spot.
- **Step 3** The foam edge points were calibrated by searching for the smallest grey value points in the edge interval of the next spot, and we used the edge points of the light spot as a starting point to form the foam edge point set.

The edge of the light spot is shown in Fig. 4(b). As shown in Fig. 4(c), the light spot edge could be used to effectively obtain the bubble edge point set by searching for surrounding bubble edge points.
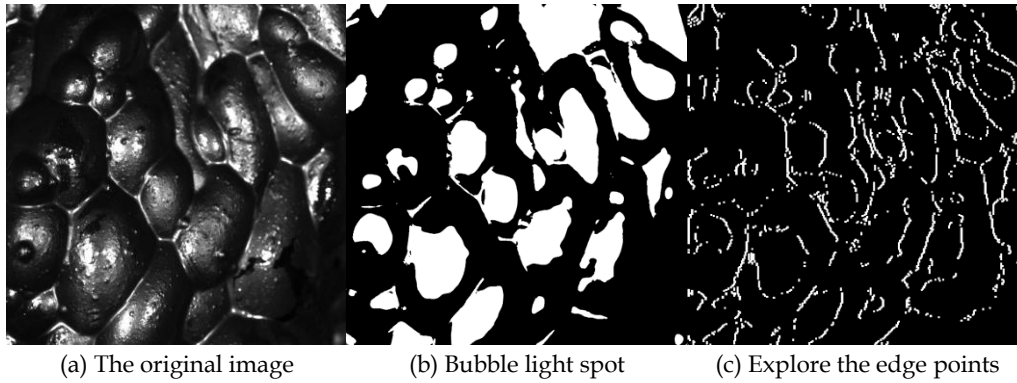
(a) The original image   (b) Bubble light spot   (c) Explore the edge points

Fig. 4. Foam edge point acquisition

2.3.2. Pseudo-edge point removal

After the above operations, numerous edge points were obtained. As shown in Fig. 8(d), a large number of pseudo-edge points were still present in the point set. In this work, we proposed a region and spatial removal algorithm to remove the pseudo-edge points by exploiting the relationship between region and space. The current edge point was defined as the decision point, and region removal was based on the local region. If the greyscale information of the area where the decision point was located conformed to the non-candidate point state, the decision point would be removed from the edge point set. Space removal was based on the spatial position of the decision point to determine the spatial relationship between the decision point and other edge points, and if it conformed to the non-candidate point state, the decision point was removed from the set of edge points.

2.3.2.1. Region removal

To better perform Region removal, in this study, we defined the region removal operator:

$$K_1 = \begin{pmatrix} 1 & 1 & 1 \\ 1 & 0 & 1 \\ 1 & 1 & 1 \end{pmatrix}. \tag{1}$$

The preprocessed image was convolved (Pang et al., 2017), and the grey value of the convolved feature layer was determined, where the greyscale information of the area where each decision point was located and counted, and when the greyscale value was greater than the specified greyscale value, the decision point was considered a pseudo-foam edge point in the center of the foam, and the point was removed from the edge point set. When the operator and feature layers performed convolution operations, the neighborhood weights of the points were preferentially determined, and the grey values of the determined points themselves did not participate in the grey value computation, which could reduce the impact on the determination results.

The region removal algorithm had the best effect on the removal of pseudo-edge points in the central area of foam or the existence of tiny dark areas caused by coal particle bulges. The results are shown in Fig. 8(e), where a good screening effect was achieved under the condition of sacrificing some accurate candidate points.

2.3.2.2. Spatial removal

There were still some pseudo-edge points in the edge point set after region removal. In this study, we used the spatial removal algorithm to screen the foam edge points again for the set of edge points after region removal. Spatial removal determined the spatial relationship between the decision point and the other edge points, and if it conformed to the non-candidate point state, the decision point was removed from the set of edge points. Subsequently, the shortest distance between the decision point and the other edge points was calculated. When the shortest distance was greater than the specified maximum value, the decision point was considered to be a pseudo-edge point, and the point was cleared from the set of edge points to generate a set of candidate points.

Region removal offers high execution efficiency, low time complexity, and low precision, and has shown to be suitable for rough screening of a large number of edge points. Spatial removal offers a low execution efficiency, high time complexity, and high precision, and has shown to be suitable for fine screening with few edge points (Pierre et al., 1986). In this study, we first showed that the region removal algorithm could be used to screen the set of edge points for the first time, and the number of screened edge points was reduced. Then, the spatial removal algorithm was used to fine-tune screen the edge points, and the combination of region removal and spatial removal algorithm could ensure high accuracy and improve the efficiency of the algorithm. As shown in Fig. 8(f), the candidate point set after removing the pseudo-edge point met the experimental requirements.

2.3.3. Double-point directional extension

The candidate points in the selected candidate point set were in a discontinuous state, and it was difficult to describe the characteristic information of the foam image. Therefore, in this study, we proposed a double-point directed continuation algorithm to extract the edges of the foam image. Due to the presence of numerous dark areas in a foam image, when a traditional extension algorithm detects the candidate points to the periphery and undergoes extension, it can easily lead to the accumulation of new edge candidate points; therefore, this can fail to form an effective segmentation edge and the image is under-segmented. In this study, we proposed a double-point directional extension scheme to effectively solve this problem.

We defined the double-point directional extension operator according to:

$$K_2 = \begin{pmatrix} 1 & 1 & 1 \\ 1 & 9 & 1 \\ 1 & 1 & 1 \end{pmatrix}. \tag{2}$$

The candidate point set after spatial removal was convolved with K_2, the grey value of the convolutional feature layer was determined, and all of the pixels in the candidate point set were classified, which could be divided into isolated-point, extended-point, non-extended-point, and the background. The operator gave priority to the weight of decision points and determined the result of convolution, where the point with a grey value $9*255$ was defined as an isolated point, with no other candidate points in the neighborhood of the determination point, and it had to be converted into an extension point later. Pixels with a grey value $10*255$ were defined as extension points, with a single candidate point in the decision point neighborhood, which was subsequently used for a double-point directional extension to obtain the new foam edge candidate points. Pixels with a grey value greater than $10*255$ were defined as non-extended points, with multiple candidate points in the neighborhood of the decision point, and there was no need to extend to the periphery. Pixels with a grey value less than $9*255$ were defined as the background. The operator could effectively classify each pixel in the image, and the corresponding subsequent operations were carried out for four different types of point sets; thus, improving the execution efficiency.

Due to the limitations of the traditional edge extension algorithm, when exploring the surrounding area, the smallest point in the neighborhood was selected as the new edge candidate, and the accumulation of new foam edge candidate points could easily occur in the process of foam image edge extension. The double-point extension algorithm proposed in this work predicted the position of the next candidate point for the extension point and the candidate point of the foam edge in its neighborhood. Fig. 5 shows the eight directional extension schemes, where the extended-point was O and the other edge candidate points in the neighborhood were H, and the corresponding directional extension scheme was selected according to the relative position of the double points to explore the X area, to find and calibrate new foam edge candidate points in the candidate point set, and this process was iterated to complete the extraction of the foam edges.

There were no other foam edge candidate points in the neighborhood of the isolated point; therefore, a directional extension could not be performed. As a result, the isolated point first explored the new foam edge candidate points in the neighborhood, which were marked in the candidate point set. After converting to an extension point, subsequent operations were completed according to the double-point directional extension algorithm.

The candidate point set after the double-point directional extension is shown in Fig. 8(g). As shown in Fig. 8, the double-point directional extension algorithm effectively solved the new candidate point accumulation and under-segmentation problems in the foam edge candidate point extension process. Therefore, the final segmentation edge was consistent with the actual bubble edge, and the continuity of the boundary was guaranteed.

```
X X X       X X  H       X        H
    O X  H  O X       O X  X  O  X
H       X       X X  X  X  X  X  X  X

X       H  X X       X  X  X  X  X  X
X  O        X  O H  X  O       X  O  X
X  X  X  X  X       X        H        H
```

Fig. 5. Directional extension scheme

3. Segmentation effect determination standard

The traditional segmentation effect determination standard (Zheng Z et al., 2020) determined the final segmentation effect by calculating the overlapping ratio of the segmented area and the real area, which consisted of the ratio of their intersection and union, according to:

$$P = \frac{F_u \cap F_v}{F_u \cup F_v} * 100\% \tag{3}$$

where F_u is the area occupied by the algorithm segmentation edge points, F_v is the area occupied by the manual segmentation edge points, and P is the final determination result, where, $F_u \cap F_v$ represents the number of overlapping pixels of the edge segmented by algorithm segmentation and manual segmentation, and $F_u \cap F_v$ represents the number of the union of the edge pixels segmented by algorithm segmentation and manual segmentation. The final segmentation effect was determined by calculating the ratio information.

(a) The original image   (b) Watershed   (c) Canny
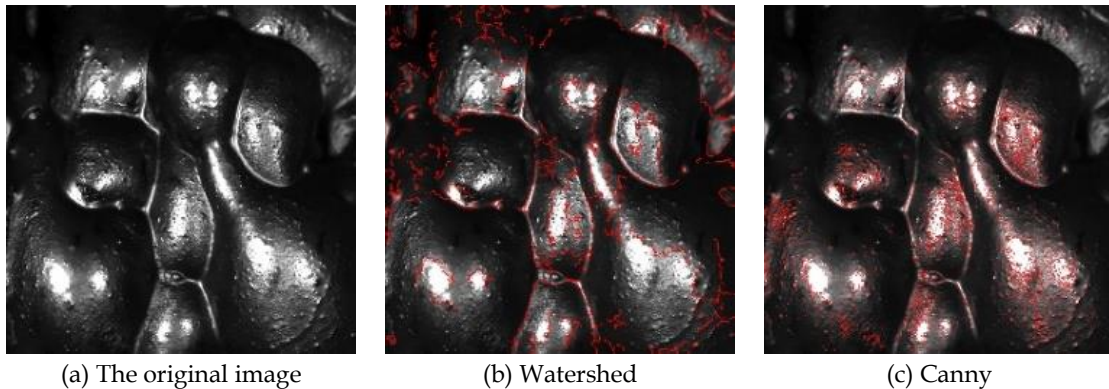
Fig. 6. Traditional segmentation algorithm segmentation comparison graph

Because the bubbles in the slime foam images adhered to each other, the extracted edges were narrow and not obvious. The traditional segmentation effect determination standard only considered the proportion of the segmentation area, while foam image segmentation only obtained the edge information, resulting in a large error in the final determination result.

As shown in Fig. 6, the values of superposition in the segmented region and the real region were calculated, as shown in Table 1, and according to Eq. 3, the Canny results were higher than those of the watershed algorithm. The segmentation effect of the Canny algorithm was better than the watershed algorithm, and the actual edge extraction effect through the watershed algorithm was slightly better than the Canny algorithm. From the above experiments, we found that in the coal slime foam image, the calculation results of the traditional segmentation criteria were inconsistent with the actual segmentation effect, and the traditional criteria had limitations in this determination object.

Table 1. Comparison of algorithms for traditional criteria

	Watershed	Canny
$F_u \cap F_v$	5231	8848
$F_u \cup F_v$	9544	13367
P	54.809%	66.193%

Considering the limitations of traditional criteria for determining the separation effect of the slime flotation foam, a new criterion for determining separation was proposed in this work. In addition to considering the segmentation of the object ontology, the criterion also included the background of the criterion and assigned weights to the segmentation area and the background area to improve the accuracy of the final determination:

$$P = (2c \frac{F_u \cap F_v}{F_u + F_v} + 2(1 - c) \frac{B_u \cap B_v}{B_u + B_v}) \times 100\% \tag{4}$$

where F_u is the area occupied by the edge points of the algorithm segmentation, F_v is the area occupied by the edge points of manual segmentation, B_u is the background area of the algorithm segmentation, B_v is the background area of the manual segmentation, c is the weight value with a value range of $0 - 1$, P is the result of final determination, $F_u \cap F_v$ represents the number of overlapping pixels of the edge segmented by algorithm segmentation and manual segmentation, $F_u + F_v$ represents the sum of the edge pixels segmented by algorithm segmentation and manual segmentation, $B_u \cap B_v$ represents the overlapping number of background pixels between algorithm segmentation and manual segmentation, and $B_u + B_v$ denotes the sum of algorithm segmentation and manual segmentation of the background pixels. By adding weight values for the segmented region and the background, the ratio information was calculated to determine the final segmentation effect.

As an example, as shown in Fig. 6, the calculation results using the segmentation effect determination standard proposed in this work are presented in Table 2. As indicated in the table, the watershed algorithm was 1.457% higher than the Canny algorithm, and the segmentation determination result of the watershed algorithm was better than the Canny algorithm, which was consistent with the actual segmentation effect. Therefore, the segmentation effect criterion proposed in this work was superior to the traditional segmentation effect criterion.

Table 2. Comparison of algorithms used for the proposed criterion in this work

|	Watershed	Canny
$F_u \cap F_v$	925	619
$F_u + F_v$	7755	5264
$B_u \cap B_v$	80456	76633
$B_u + B_v$	169531	165914
P	59.386%	57.929%

In addition to verifying the effect of edge detection and segmentation, this criterion could also verify the effect of instance segmentation. Compared to the traditional verification method, the background was added as a reference to the original basis, and weights were added to different segmentation objects to determine the segmentation effect, with information that was more inclined to a particular object, and the criterion for determining the segmentation effect was universal.

4.   Analysis of the results

4.1. Source of the image set

The foam images used in this study were collected by a coal-washing company in the Inner Mongolia Autonomous Region. The collection device mainly consisted of a camera, light source, equipment boxes, and storage devices, as shown in Fig. 7. The camera model was an industrial camera MV-E800M, and

the light source consisted of a double 8000 K 40 W spotlight. The equipment box was shielded from light to ensure that it was not affected by external light sources when collecting the foam images. The method involved taking foam images of flotation tanks No. 1 and No. 2 every 2 s, collecting 500 cm³ of the foam layers in flotation tanks No. 1 and No. 2 every 20 min, and collecting 1 dm³ of raw coal and tail coal every 30 min, for 11 h a day for 8 days in total.
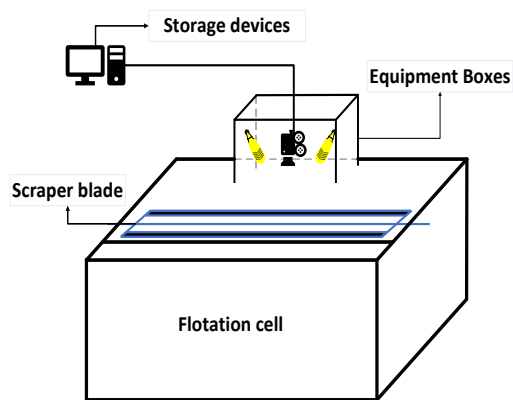
(a) Design of the acquisition equipment   (b) Field image acquisition

Fig. 7. Foam image acquisition

4.2. Experimental results

Four different types of foam images were selected. As shown in Fig. 8, the surface of foam image 1 was large with coal particles, contained a lot of noise, and had a large area covered by light spots. Foam image 2 had a large bubble area and uniform surface texture. Foam image 3 contained severe dark regions and non-obvious edge boundaries. In foam image 4, the bubbles were dense and small, and the dark area was severe. Considering the above four different scenes, the proposed segmentation algorithm could achieve good edge extraction results.

First, after preprocessing the original image, the noise in the original image and the shadow on the surface of the foam caused by the uneven size of the coal particles were eliminated. As shown in (b), the pre-processed image had a clear boundary, smooth bubble surface, and no obvious noise, with a good preprocessing effect.

Second, the improved FCM clustering algorithm was used to divide the processed image into regions, and the divided regions ewer obtained through image binarization and morphological operations, while the obtained light spot edge, as shown in (c), was consistent with the actual light spot edge.

Third, we took the edge of the light spot as the starting point to explore the foam edge points to the periphery, and as indicated in (d), the foam edge point set could be accurately extracted.

Then, due to the presence of many pseudo-edge points in the edge point set, we proposed region and spatial removal algorithms. The filtered candidate point set is shown in (f), where the pseudo-edge points in the central area of the bubble were eliminated, and the filtering effect was good.

Finally, the pixels of the candidate point set feature map after cleaning were classified into the isolated point, extended point, non-extended point, and background. A double-point directional

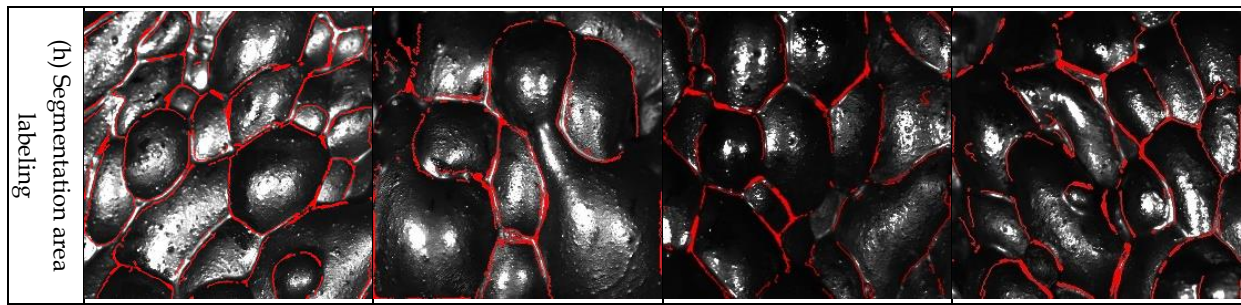|	Image 1	Image 2	Image 3	Image 4
(a) The original image				
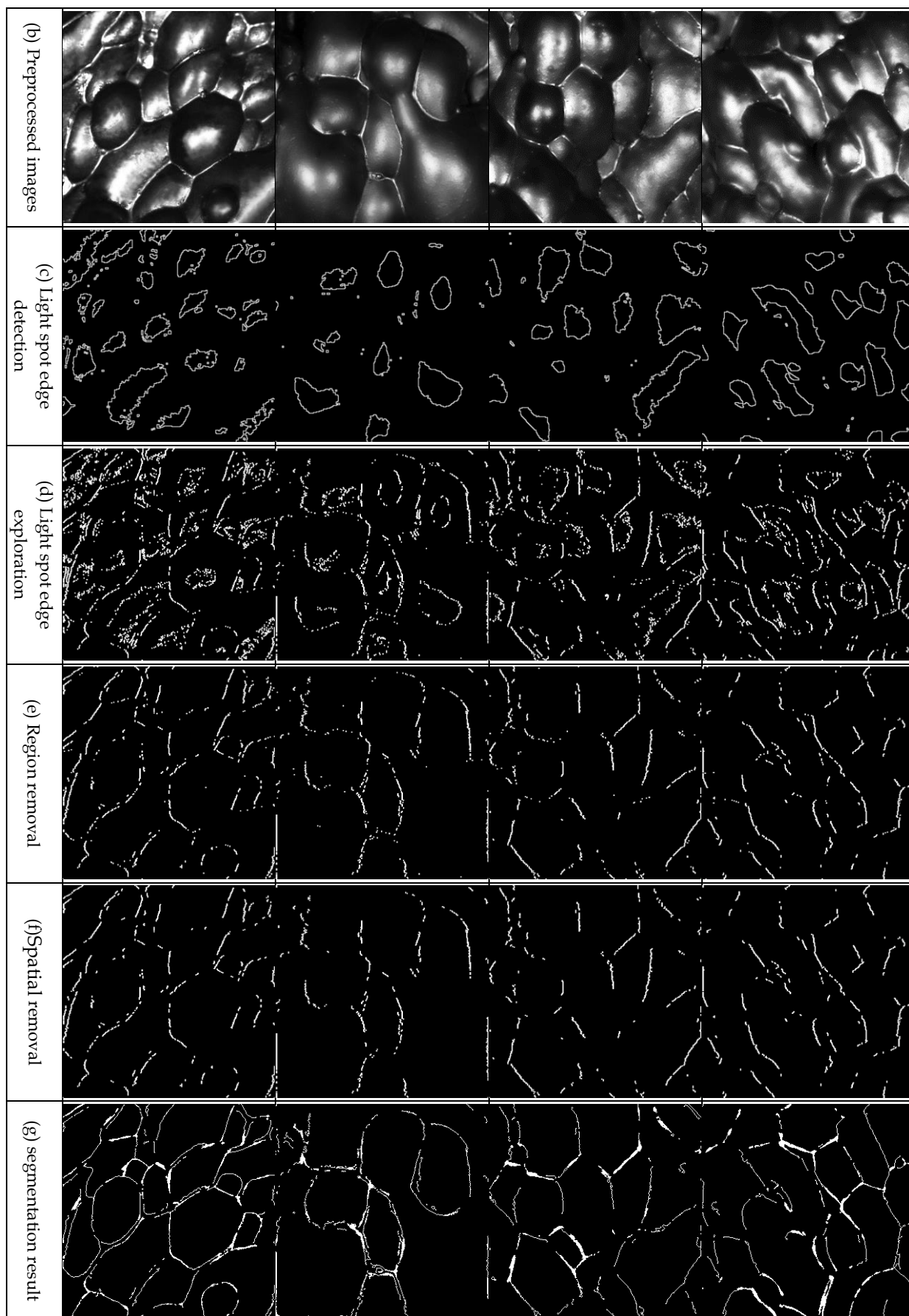
Fig. 8. Experimental results

extension algorithm was used to extract the foam edges by extending into the neighborhood, and the final segmentation results are shown in (g). As indicated by the labeling map in (h), the segmentation area of the edge extracted by the algorithm in this work was consistent with the actual edge of the original image, and we could determine that the algorithm proposed in this work had a good segmentation effect.

4.3. Comparative analysis

Figure 9 shows the segmentation results of the several algorithms used for the two different foam images. We observed a large gradient in the grey-scale variation of the bubble light spot, with a wide gradient in the dark region at the bubble edge, and a small gradient in the grey-scale variation. The watershed algorithm over-segmented the edge of the bubble light spot and under-segmented the edge
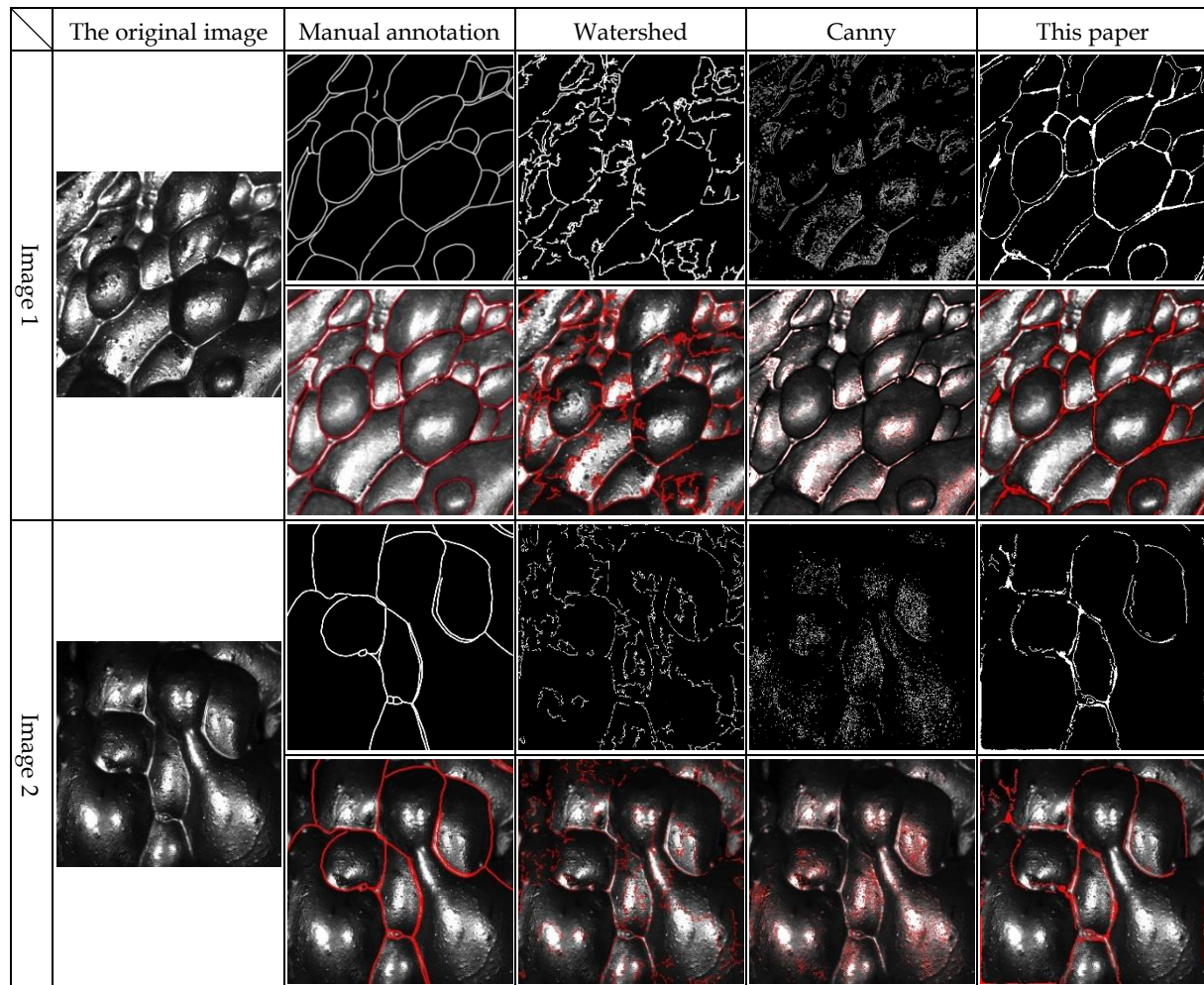

Fig. 9. Comparison of segmentation effect

segmentation, and the gradient change in the light spot of the foam image was the largest; therefore, the segmentation edge mainly occurred at the edge of the light spot instead of the edge of the bubble. The proposed double-point directed continuation algorithm could efficiently solve the above problem and extract the foam edge.

Based on the segmentation results of the foam images, the relevant variables of the segmented regions were measured using the proposed segmentation effect determination criterion, resulting in the pixel statistics of the regions, which were then measured for the manually segmented images. Each value was calculated according to the determination criterion proposed in this work. Taking the two images in Fig. 9 as an example, the results of segmentation judgment under different algorithms were subsequently calculated.

Table 3. Comparison of the determination effect

	Image 1			Image 2		
	Watershed	Canny	This paper	Watershed	Canny	This paper
$F_u \cap F_v$	3746	1243	5246	925	619	1380
$F_u + F_v$	23356	15589	21648	7755	5264	9749
$B_u \cap B_v$	67726	69450	73598	80456	76633	81631
$B_u + B_v$	153980	158207	158352	169531	165914	170251
P	60.022%	51.872%	70.711%	59.386%	57.929%	62.103%

As shown in Table 3, the algorithm proposed in this work had a higher segmentation accuracy, a better effect than traditional segmentation algorithms, and could better complete the task of image feature extraction.

Taking the two original images in Fig. 9 as examples, the iterative results of the proposed double-point directional extension algorithm and traditional extension algorithm are shown in Fig. 10. The solid line consisted of the double-point directional extension algorithm, and the dashed line was the traditional extension algorithm. With an increase in the number of iterations, the segmentation accuracy of the double-point directional extension algorithm continued to improve, and finally became stable. However, the segmentation accuracy of the traditional extension algorithm was low, the segmentation accuracy of the iterative process fluctuated greatly, and the overall segmentation accuracy was lower than the double-point directional extension algorithm. Finally, we concluded that the segmentation algorithm proposed in this work was more effective.
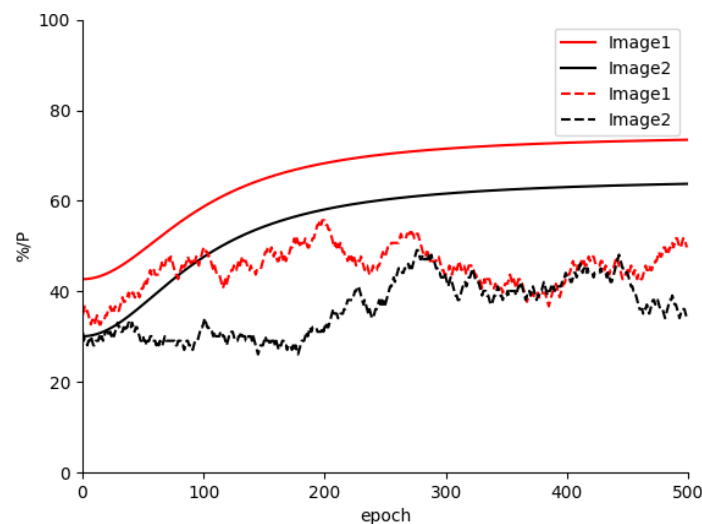

Fig. 10. Extended segmentation effect iteration curve

5. Conclusions

In this work, a double-point extended slime foam image segmentation algorithm based on improved FCM clustering was proposed to address the difficulty faced by traditional segmentation algorithms in

accurately segmenting slime foam due to adhesion and a fuzzy boundary. The experimental results showed that the double-point directional extension algorithm had the characteristics of fast and high accuracy, and achieved a good segmentation effect for the slime foam image. In this study, the new foam edge points were calibrated by exploring the minimum grey value points around the edges. The foam features extracted using this method could be applied to the identification of flotation production states. In addition, this method was compared with other methods and showed better performance.

Acknowledgments

References

ALDRICH, C., FENG, D. 2000. *Effect of frothers on bubble size distributions in flotation pulp phases and surface froths*. Minerals Engineering, 13(10), 1049-1057.

ALDRICH, C., MARAIS, C., SHEAN, B.J., CILLIERS, J.J. 2010. *Online monitoring and control of froth flotation systems with machine vision: A review*. International Journal of Mineral Processing, 96(1-4):1-13.

ARYASUTA, N., JENA, M.S.& MANDRE, N.R. 2022. *Beneficiation of lead-zinc ores – A Review*, Mineral Processing and Extractive Metallurgy Review, 43:5, 564-583.

BACKES, A.R., CASANOVA, D., BRUNO, O.M. 2013. *Texture analysis and classification: A complex network-based approach*. Information Sciences, 219(Complete), 168-180.

BHONDAYI, C. 2022. *Flotation froth phase bubble size measurement*. Mineral Processing and Extractive Metallurgy Review, 43:2, 251-273.

CAO, W., QIAO, Z., GAO, Z., LU, S., TIAN, F. 2021. *Use of unmanned aerial vehicle imagery and a hybrid algorithm combining a watershed algorithm and adaptive threshold segmentation to extract wheat lodging*. Physics and Chemistry of the Earth, Parts A/B/C, 123, 103016.

CHO, Y.S., LASKOWSKI, J.S. 2002. *Effect of flotation frothers on bubble size and foam stability*. International Journal of Mineral Processing, 64(2-3), 69-80.

CHUDASAMA, D., PATEL, T.A., JOSHI, S., PRAJAPATI, G. 2015. *Image segmentation using morphological operations*. International Journal of Computer Applications, 117(18).

DENG, Q., ZHAN, Y., LIU, C., QIU, Y., ZHANG, A. 2021. *Multiscale power spectrum analysis of 3D surface texture for prediction of asphalt pavement friction*. Construction and Building Materials, 293, 123506.

DENIZ, V., UMUCU, Y., DENIZ, O.T. 2022. *Estimation of grade and recovery in the concentration of barite tailings by the flotation using the MLR and ANN analyses*. Physicochemical Problems of Mineral Processing, 58(5).

FENG, S. 2022. *Effective document image binarization via a convex variational level set model*. Applied Mathematics and Computation, 419, 126861.

GARCÍA-FERNÁNDEZ, Á.F., RALPH, J., HORRIDGE, P., MASKELL, S. 2021. *A Gaussian filtering method for multitarget tracking with nonlinear/non-Gaussian measurements*. IEEE Transactions on Aerospace and Electronic Systems, 57(5): 3539-3548.

HAN, S., XI, S., GENG, W. 2017. *Low-resolution expression recognition based on central oblique average CS-LBP with adaptive threshold*. Optoelectronics Letters, 13(6), 444-447.

HE, D.C., WANG, L. 1990. *Texture unit, texture spectrum, and texture analysis*. IEEE Transactions on Geoscience and Remote Sensing, 28(4), 509-512.

HUIFENG, R., CHUNHUA, Y., XUAN, Z., WEIHUA, G., FENG, Y. 2011. *Morphological characteristics extraction of mineral flotation froth based on adaptive edge detection*. Control and Instruments in Chemical Industry, (7), 5.

JING, J., LIU, S., WANG, G., ZHANG, W., SUN, C. 2022. *Recent advances on image edge detection: A comprehensive review*. Neurocomputing.

JIAN, L., JIUSI, W., JIANGPING, L., AIPING, K., YANLING, J. 2008. *Application of surfactants in foam flotation separation*. Advances in Fine Petrochemicals, 9(6), 4.

JING, W., SHUTING, C., SHIYIN, L., ZHAOLIN, L. 2017. *Research on image segmentation algorithm of coal flotation froth*. Coal Technology, (3):3.

JONES, R., SVALBE, I. 1994. *Algorithms for the decomposition of gray-scale morphological operations*. IEEE Transactions on Pattern Analysis and Machine Intelligence, 16(6), 581-588.

JOSE, F. O. & RUPEN, A. 1992. *Physico-chemical factors affecting the separation of cassiterite and fluorite by froth flotation*. Mineral Processing and Extractive Metallurgy Review, 9:1-4, 125-134.

JUN, Z., CHAO, W., SHUAI, W., WEI, H. 2020. *Combining improved watershed algorithm with k-means method in image segmentation*. Journal of Chongqing University of Technology (Natural Science), 34(4), 7.

KAIJUN, Z. 2010. *Froth image morphological characteristic extraction method and its application for mineral flotation*. Central South University.

KARUNKUZHALI, D., MEENAKSHI, B., LINGAM, K. 2022. *An adaptive fuzzy c means with seagull optimization algorithm for analysis of WSNs in agricultural field with IoT*. Wireless Personal Communications, 1-22.

KIM, H., AHN, E., CHO, S., ET AL. 2017. *Comparative analysis of image binarization methods for crack identification in concrete structures*. Cement and Concrete Research, 2017, 99, 53-61.

LAVANYA, D.N., THIRUMURUGAN, P. 2022. *Cervical cancer classification from pap smear images using modified fuzzy C means, PCA, and KNN*. IETE Journal of Research, 68(3), 1591-1598.

LIKAS, A., VLASSIS, N., VERBEEK, J.J. 2003. *The global k-means clustering algorithm*. Pattern recognition, 36(2): 451-461.

LIU, Y.Y., LI, Y.P., ZHU, T.T, ET AL. 2011. *Imaging study of surfactant effect on bubble behaviors in froth flotation*. International Symposium on Water Resource and Environmental Protection. IEEE, 2, 1199-1202.

LUO, J., TANG, Z., ZHANG, H., FAN, Y. 2019. *A new flotation froth texture feature extraction method based on PCA*, IEEE Symposium Series on Computational Intelligence (SSCI). IEEE.

MENG, F., WANG, X., SHAO, F., WANG, D., YU, Y.W., XIAO, Y. 2021. *Visual-attention gabor filter based online multi-armored target tracking*. Defence Technology, 17(4), 1249-1261.

MURPHY, D.G., ZIMMERMAN, W., WOODBURN, E.T. 1996. *Kinematic model of bubble motion in a flotation froth*. Powder Technology, 87(1), 3-12.

NAKHAEI, F., IRANNAJAD, M., MOHAMMADNEJAD, S. 2019. *Column flotation performance prediction: PCA, ANN and image analysis-based approaches*. Physicochemical Problems of Mineral Processing, 55.

NG, H.P., ONG, S.H., FOONG, K.W.C., GOH, P.S., NOWINSKI, W.L. 2006. *Medical image segmentation using k-means clustering and improved watershed algorithm*. IEEE southwest symposium on image analysis and interpretation. IEEE, 61-65.

PANG, Y., SUN, M., JIANG, X., LI, X. 2017. *Convolution in convolution for network in network*. IEEE transactions on neural networks and learning systems, 29(5), 1587-1597.

PARK, H., BAI, C., WANG, L. 2022. *A convolutional neural network for classification of froth mobility in an industrial flotation cell*. Mineral Processing and Extractive Metallurgy Review, 1-9.

PARK, H., NG, C.Y., WANG, L. 2022. *Bubble size in a flotation column with oscillatory air supply in the presence of frothers*[J]. Mineral Processing and Extractive Metallurgy Review, 43(7), 926-934.

PIERRE, D.A. 1986. *Optimization theory with applications*. Courier Corporation.

SI, S.H., HU, F.Y., GU, Y.J., XIAN, X.F. 2014. *Improved denoising algorithm based on non-regular area Gaussian filtering*. Computer Science, 41, 313-316.

SU, Z., LIU, W., YU, Z., HU, D., LIAO, Q., TIAN, Q., PIETIKAINEN, M., LIU, L. 2021. *Pixel difference networks for efficient edge detection*. Proceedings of the IEEE/CVF International Conference on Computer Vision. 5117-5127.

UPLAONKAR, D.S., PATIL, N. 2021. *Ultrasound liver tumor segmentation using adaptively regularized kernel-based fuzzy C means with enhanced level set algorithm*. International Journal of Intelligent Computing and Cybernetics.

KALYANI, V.K., PALLAVIKA, SANJAY CHAUDHURI, GOURI CHARAN, T., HALDAR, D.D., KAMAL, K.P., BADHE, Y.P., TAMBE, S. S. & KULKARNI, B.D. 2007. *Study of a laboratory-scale froth flotation process using artificial neural networks*. Mineral Processing and Extractive Metallurgy Review, 29:2, 130-142.

VALLEBUONA, G., CASALI, A., RODRÍGUEZ, F., ENDARA, D. 2008. *Bubbles size distribution in mechanical flotation cells at laboratory and industrial scale and modeling of the effects of the operating variables*. Revista De Metalurgia, 44(3), 233-242.

WANG, F., WANG, Y., LU, M., ET AL. 2001. *Bubble feature extracting based on image processing of coal flotation froth*. Zhongguo Kuangye Daxue Xuebao (Journal of China University of Mining and Technology), 30.

WANG, G., HE, T., KUANG, Y., LIN, Z. 2020. *Optimization of soft-sensing model for ash content prediction of flotation tailings by image features tailings based on GA-SVMR*. Physicochemical Problems of Mineral Processing, 56(4).

WANG, W., WANG, L. 2000. *Froth image segmentation algorithms and their validation*. WCC 2000-ICSP 2000. 5th International Conference on Signal Processing Proceedings. 16th World Computer Congress 2000. IEEE, 3, 2042-2045.

YUAN, B., XIA, B., ZHANG, D. 2018. *Polarization image texture feature extraction algorithm based on CS-LBP operator*. Procedia Computer Science, 131:295-301.

ZHENG, Z., WANG, P., LIU, W., LI, J., YE, R., REN, D. 2020. *Distance-IoU loss: Faster and better learning for bounding box regression*. Proceedings of the AAAI conference on artificial intelligence. 34(07), 12993-13000.

ZHOU J, YANG M. 2022. *Bone region segmentation in medical images based on improved watershed algorithm*. Computational Intelligence and Neuroscience, 2022.

ZIOU, D., TABBONE, S. 1998. *Edge detection techniques-an overview*. Pattern Recognition and Image Analysis C/C of Raspoznavaniye Obrazov I Analiz Izobrazhenii, 8, 537-559.